Materials and Design Selection to Improve High Current Density Performance in PEMFC

N. Ramaswamy[a], and S. Kumaraguru[a]

[a] Global Fuel Cell Business, General Motors Corporation, Pontiac, MI 48340, USA

Performance at high current density is dominated by transport losses from resistance to oxygen and proton transport. The materials selection and their properties can have a significant impact on the transport resistance. In this study, the impact of catalyst carbon support microstructure and its properties impacting performance at high current density is studied in detail. Platinum-cobalt alloy catalysts supported on different carbon supports were analyzed for pore size distribution characteristics. Catalyst layer electrochemical diagnostics such as oxygen limiting current and H_2/N_2 impedance tests were conducted to measure local oxygen transport resistance and bulk proton transport resistance. For the first time, the local-oxygen transport and the bulk-proton transport resistances in the catalyst layer are directly correlated to the micropore and macropore properties of the carbon support.

Introduction

Current state of the art PEMFC cathode catalyst layers can be described as a complex, heterogeneous porous system with multiple components across various length scales at which both the electrochemical reaction and mass transport of reactants/products occur. The functional components in the catalyst layer consist of the platinum catalyst nanoparticles (few nm in diameter) for electrochemical reaction, carbon support (few tens of nm to µm) for electron conduction, ionomer chains (few nm to µm) for proton transport, and pore volume (few nm to few hundred nm) for gas transport. Mass transport of reactants and products are supported by the intrinsic pore structure in the carbon support and the secondary pore structure induced by the ionomer chains in the catalyst ink formulation stage. [1]

There is a strong impetus to decrease the platinum loading in the catalyst layer to reduce cost and ease the supply-demand of Pt. While extensive research into the development of highly active Pt-alloy nanoparticle catalyst systems has led to tremendous improvements in the low current density kinetic performance region, the current state of the art cathode suffers from poor high current density (HCD) performance at low Pt loadings which leads to an increase in stack area and cost. This brings into focus the need to fundamentally understand the functional role and microstructure-property relationships of the various components in the cathode catalyst layer towards mitigating the HCD mass transport losses at low platinum loading. [2]

Recent studies have pointed to the presence of a local transport resistance in the cathode catalyst layer that affects high current density performance via i) decrease in O_2 permeability through the ionomer thin film covering the Pt/C agglomerates, and/or ii) O_2 transport within the Pt/C agglomerates. The latter resistance arises due to the necessity of O_2 to be transported within the tortuous pore structure within the Pt/C agglomerates to reach the active site. [2, 3] Perhaps the most complex aspects of the catalyst layer microstructure arise from i) aggregated pore structure of the carbon support upon which the Pt-alloy nanoparticles are deposited, and ii) extensive aggregation of the colloidal ionomer particles. A well optimized cathode catalyst layer could be envisioned as one where the ionomer is distributed around the Pt/C particles with an optimal coverage in such a fashion that there is no direct Pt-ionomer interface formation (to minimize sulfate poisoning), but with Pt nanoparticles present at vantage locations within the agglomerates that are more open, less tortuous and easily accessible by O_2. Such a structure would essentially maximize the mass activity in the kinetic regime and minimize the local-O_2 transport resistance in the mass transport regime.

In this study, we systematically evaluate the impact of carbon support pore structure distribution on the high current density transport resistances. Specifically, we evaluate PtCo nanoparticle catalyst distributed on six different carbon black supports of varying micro-, meso-, and macro-porosity. Catalyst layer transport properties such as the local-O_2 transport and bulk-proton (H^+) transport resistances were measured in a 5 cm^2 differential cell platform. Measured transport resistances under *in situ* conditions are then correlated to the *ex situ* properties of catalyst microstructures to yield direct quantitative relationships and fundamental physical insight that affect the high current density performance.

Experimental Details

PtCo nanoparticle catalysts dispersed on six different carbon supports at a nominal content of 30% by weight was used on the cathode at a loading of 0.1 mg_{Pt}/cm^2. All anode catalyst layer consisted of a 10% Pt/C catalyst at 0.025 mg_{Pt}/cm^2. D2020 perfluorosulfonic acid (PFSA) ionomer with an equivalent weight of 950 g/mol was used in the catalyst layers at an ionomer to carbon ratio of 0.6 and 0.8 for the anode and cathode, respectively. An 18 µm thick PFSA ionomer with a reinforcement layer was used as the membrane to build 5 cm^2 active area membrane electrode assemblies (MEAs). Roughly 230 µm thick carbon-fiber-paper-based gas-diffusion layer was used on both the anode and cathode sides. Details on the fabrication of electrode and lamination of catalyst-coated membrane (CCM) MEAs can be found elsewhere. [4]

Ex situ characterization to quantify the N_2-adsorption surface area and pore size distribution of the catalyst powders was carried out using a Micromeritics Instrument Corporation ASAP 2020 Physisorption system. N_2 gas of ultrahigh purity was used and the measurements were carried out at 77 K. Total specific surface of the catalyst was determined using the Brunauer-Emmett-Teller (BET) procedure in the range of 0.05 – 0.2 N_2 partial pressure, pore-size distribution was quantified using Barrett-Joyner-Halenda (BJH) methodologies and micropore surface area was quantified using the t-plot analysis. [5] The method is based on the Kelvin equation and accounts for the formation of a condensed layer of gas molecules on the pore wall prior to capillary condensation using the Harkins-Jura equation:

$$t = (13.99/(0.034 - \log (p/p_0)))^{1/2}$$

where, *t* is the thickness of the adsorbed layer on the pore wall (Å), *p* the partial pressure of N_2, and p_0 the saturation pressure of N_2 at 77 K. A plot of the thickness of the adsorbed layer versus the volume adsorbed is called the *t*-plot. The intercept of the *t*-plot yields the micropore volume. The slope of the *t*-plot yields the total external surface area which is the sum of the meso- and macropores. Micropore area is then calculated from the difference between the total BET and external surface areas.

Electrochemical diagnostics such as CO_{ads} surface area, O_2 limiting current and H^+ transport resistances were carried out in a test fixture containing the 5 cm^2 active area MEA. Details on these measurement methods can be found elsewhere. [6, 7, 8]. Briefly, the local oxygen transport resistance ($R(O_2)$-local) was calculated using the limiting current density measurements done at low O_2 partial pressures under sub-saturated operating conditions (64 to 77% RH) at 80 °C. [6, 7] O_2 limiting current densities were measured as a function of total pressures (110 to 300 kPa_{abs}), O_2 mole fractions (0.01 to 0.04) and cathode Pt loading (0.05, 0.1, 0.2 mg_{Pt}/cm^2). The total transport resistance of the cathode electrode consists of both the pressure-dependent and pressure-independent terms. $R(O_2)$-local can be extracted from the pressure-independent portion of the resistance. First, the total transport resistance was calculated from the slope of the plot between limiting current and dry O_2 mole fraction at different total pressures mentioned above. The slope of the plot between total transport resistance and total pressure gives the pressure-dependent resistance whereas the intercept at zero total pressure yields pressure-independent resistance. Subsequently, a plot of pressure-independent transport resistance vs. the roughness factor of the catalyst layer (derived from the ECSA at various loadings) at different loadings is used to generate the $R(O_2)$-local.

Proton transport resistance of the catalyst layer was measured using a H_2/N_2 electrochemical impedance spectra (EIS) methodology as discussed in detail elsewhere. [8] This involved the flow of H_2 on the anode and N_2 on the cathode at 80 °C and various RH values from 20 % to 122 %. EIS measurement was carried out at a DC potential of 0.2 V with 0.15 mV amplitude from a frequency of 0.5 Hz to 20 kHz. EIS spectra were fit using a transmission line model from which the proton transport resistance in the membrane and the cathode catalyst layer were obtained. [8]

Results and Discussion

PtCo nanoparticle catalyst dispersed on six different carbon supports were investigated in this work. The carbon black supports were classified based on their surface area and are labeled as HSC-a, HSC-b, HSC-e, HSC-f, HSC-g and MSC-a where HSC and MSC stand for high-surface-area carbon and medium-surface-area carbon, respectively. Catalyst powders were characterized using N_2 physisorption measurements followed by analysis of the surface area and pore size distribution using the Brunauer-Emmett-Teller (BET) and Barrett-Joyner-Halenda (BJH) methodologies. Figure 1a shows the N_2 adsorption pore size distribution of PtCo nanoparticle catalysts on six different carbon supports that have been investigated in this study. The BET surface area and pore size distribution of the catalysts on various carbon supports are summarized in Table 1.

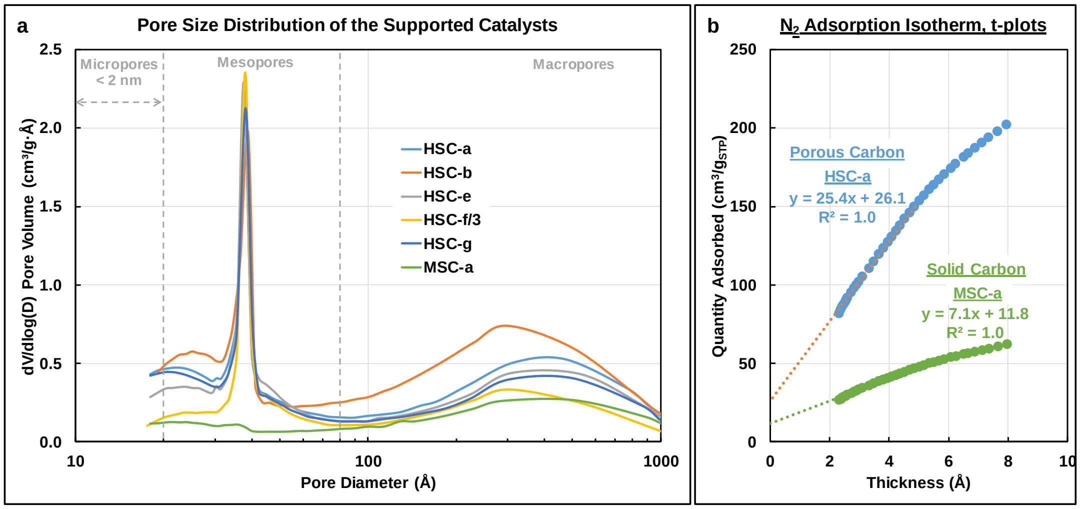

Figure 1. BET-BJH N_2-adsorption measurements of the PtCo catalysts supported on various carbon black materials used in this study showing (a) the pore-size distribution and (b) the t-plots used to calculate the micropore surface area.

Table 1: Surface areas of the catalysts on various carbon supports quantified using N_2-adsorption measurements

Catalyst	BET – BJH Surface Area (m^2/g)		
	Total Surface Area (m^2/g carbon)	**Micropore (< 2 nm) (m^2/g catalyst)**	**Macropore (> 8 nm) (m^2/g catalyst)**
HSC-a	~778	79	57
HSC-b	~797	42	89
HSC-e	~778	65	49
HSC-f	>780	54	115
HSC-g	~744	82	46
MSC-a	~214	35	33

According to the general IUPAC definition, regions of adsorption can be classified as micropores (< 2 nm), mesopores (2 – 50 nm), and macropores (> 50 nm). [9] However, it is difficult to deconvolute the carbon pore structure according to this strict definition for all applications including fuel cell catalysts. As seen in Figure 1a, HSC catalysts feature a sharp increase in pore volume around ~4 nm followed by a minimum at around ~8 nm. This is then followed by an increase in volume adsorbed above 8 nm. Carbon micropores (< 2 nm), although below the detection limit of typical N_2 physisorption measurements, are known to exist in the carbon primary particles which are themselves ~30 – 50 nm in diameter. In this context, the pore size distribution shown in Figure 1a is hence divided loosely into three different regions for our application here – micropores (< 2 nm), mesopores (2 to 8 nm) and macropores (> 8 nm).

The micropore surface area (S_{micro}) can be quantified from the slope of the *t*-plot shown in Figure 1b which is a plot of the volume of gas adsorbed versus statistical thickness of the adsorbed film. According to the equations below:

$$S_{micro} = S_{BET} - S_{ext.}$$

where, S_{BET} is the total BET area of the catalyst and S_{ext} is the surface area of all pores greater than 2 nm which can be calculated as follows:

$$S_{ext} = (V_{ads}/t)(V_m P_a)/RT$$

where, the term (V_{ads}/t) represents the slope of the *t*-plot in the region 3.5 to 5 Å represented in units of (cm^3/g/Å), V_m is the molar volume of the liquid N_2 adsorbate which is equal to 34.7 cm^3/mol for nitrogen, P_a is the ambient pressure (Pascal), R is the universal gas constant (8.314 J/mol. K), and T is the ambient temperature (K).

The total surface area of different carbon supports and pore size distribution of the different catalysts are shown in Table 1. The carbon supports evaluated in this study feature total surface area ranging from ~200 m^2/g to ~ 800 m^2/g resulting in catalysts with varying combination of micro-, meso- and macro-porous regions. For instance, the HSC-a catalyst carbon support and HSC-b catalyst carbon support have comparable total BET surface area, but varying degrees of micro- and macroporous area for the catalyst. The HSC-a exhibit lower macropore and higher micropore area, whereas HSC-b exhibit lower micropore and higher macropore area. The HSC-b micropore area is comparable to much lower surface area carbon such as medium surface area carbon, MSC-a. The micropores and macropores contribute only ~10 to 25% each to the total surface area, the rest being mesoporous area that is most important to attain improved dispersion of Pt catalyst [6].

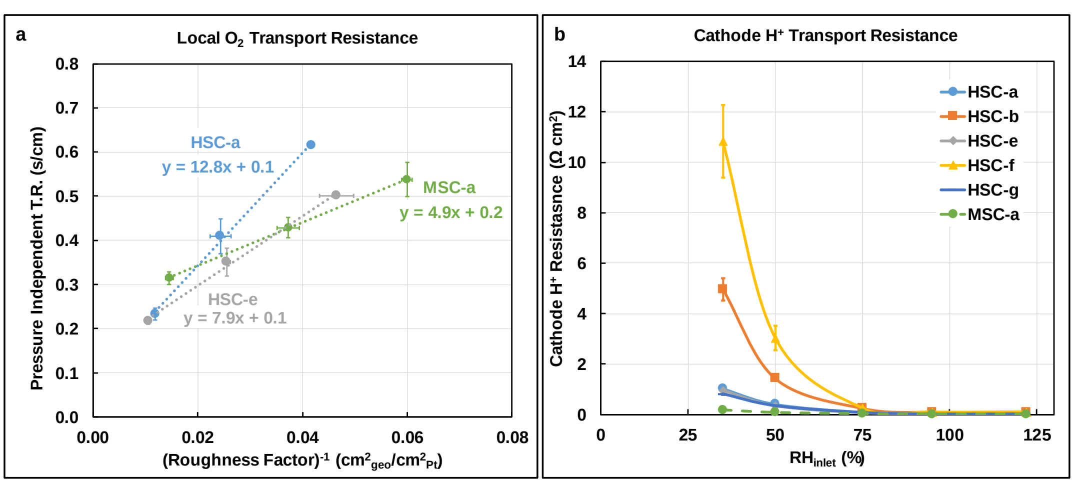

Figure 2. Plot of (a) pressure independent O_2 transport resistance vs. inverse roughness factor of the cathode catalyst layer, (b) bulk-H^+ transport resistance of the cathode catalyst layer vs. inlet relative humidity.

Figure 2a shows a plot of pressure independent O_2 transport resistance for various catalysts as a function of inverse roughness factor. As explained in the experimental section above, the slope of this plot provides a direct measure of the local-O_2 transport resistance ($R(O_2)$-local) which is a parameter that can be used to assess the resistance towards O_2 transport at or near the Pt catalyst interface. [7] This resistance could arise due to O_2 transport either through the ionomer thin film or within the porous carbon structure. As can be seen in Figure 2a, the slope of the plot is dependent on the nature of the carbon support. For instance, HSC-a catalyst features a higher slope of 12.8 s/cm whereas MSC-a catalyst features a lower slope of 4.9 s/cm. Figure 2b shows the through-plane bulk-H^+ transport resistance in the ionomer phase of the catalyst layer as a function of inlet relative humidity. While the H^+ transport resistance decreases as expected with increasing RH, the interesting part of the plot is the dependence of the resistance on the type of carbon support.

An attempt was made to derive a systematic correlation between the various pore surface areas of the catalysts and the local-O_2/bulk-H^+ transport resistances in the catalyst layer. The results of this attempt are shown in Figure 3. As shown in Figure 3a, there appears to be a direct linear correlation between the local-O_2 transport resistance and the carbon support micropore (< 2 nm) surface area. MSC-a and HSC-b catalysts featuring a low micropore surface area enables a lower $R(O_2)$-local whereas HSC-a and HSC-g catalysts with a higher micropore area show a higher $R(O_2)$-local. This indicates that the micropore openings in the carbon support could act as bottleneck to the O_2 transport in the catalyst layer. The micropores are typically suggested to exist between the edges of two graphitic crystallites in carbon primary particles that act as openings to mesoporous zones that feature the active Pt/PtCo catalyst nanoparticles. [6, 10]

Contrarily, as shown in Figure 3b the bulk-H^+ transport resistance in the through-plane direction of the catalyst layer is directly correlated to the macropore surface area (> 8 nm) of the carbon support. One factor that determines the H^+-transport in the catalyst layer is the presence of continuous, homogeneous distribution of ionomer phase around

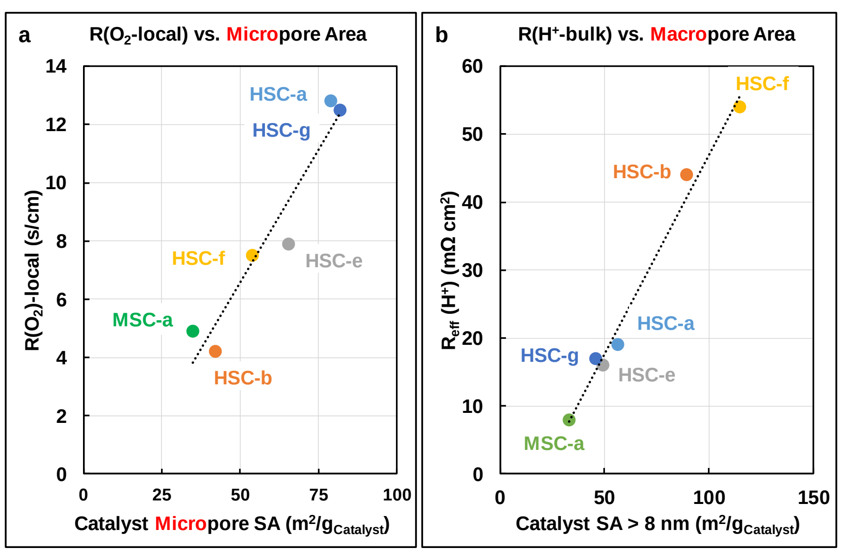

Figure 3. Plot showing the relationship between (a) local-O_2 transport resistance and catalyst micropore surface area, and (b) bulk-H^+ transport resistance and catalyst macropore area.

the carbon particles. Based on the relationship shown in Figure 3b, it appears that the macroporous surface area of the carbon support determines the uniformity and continuity of the ionomer distribution in the catalyst layer. MSC-a catalyst that features a low macropore surface area could possibly enable a more uniform and homogeneous ionomer distribution, whereas the high macropore area of HSC-f potentially disrupts such a favorable ionomer dispersion. Catalyst layer design optimization such as use of higher ionomer content can partially mitigate the bulk proton transport losses. Studies on catalyst layer structure is ongoing and will be followed through.

These results clearly indicate that the local-O_2 and bulk-H^+ transport resistance in the catalyst layer responsible for high current density performance are directly related to the fundamental structural property of the carbon black support used to disperse Pt/PtCo catalyst nanoparticles. Further, this study clearly suggests that a decrease in micropore area of the carbon support would benefit the transport of O_2 near the Pt catalyst surface, whereas a decrease in carbon macropore area would strongly benefit bulk-H^+ transport in the ionomer phase of the catalyst layer. Although not discussed here, it is noted that the overall polarization behavior will depend not only on the transport resistances but also on the kinetic properties of the catalyst nanoparticles. The significance of the mesoporous regions was not discussed in this article as they tend to primarily affect the kinetic property of the catalyst as discussed in a recent publication by Yarlagadda et al. [6] Mesoporous regions with pore sizes of ~2 to 8 nm tend to host the Pt/PtCo catalyst nanoparticles that are of average diameter ~3 to 4 nm. [10] Yarlagadda et al. suggested that porous carbons with a preferred pore opening of 4-7 nm can give catalyst layers with a high O_2 reduction reaction (ORR) kinetic activity. [6] In summary, this indicates that carbon supports that feature minimal micro- and macro-pore area along with an appreciable content of meso-pore regions would deliver catalyst layers with high ORR kinetic properties and lower local-O_2/bulk-H^+ transport resistances, and hence an improved performance across all polarization regions.

Conclusions

A systematic effort was undertaken to understand the influence of carbon black support microstructure on the reactant transport resistances (such as local-O_2 and bulk-H^+ transport) of the catalyst layer that affect the high current density performance. In this article, the focus was on identifying factors that affect the high current density transport behavior of the catalyst layer. In summary, a direct linear correlation is observed between the local-O_2 transport resistance and the microporous surface area of the carbon support. Contrarily, bulk-H^+ transport resistance was observed to be directly correlated to the macroporous surface area of the carbon support. To the knowledge of the authors, this is the first time a direct quantitative relationship has been derived relating the carbon support microstructure and the catalyst layer transport resistances that affect high current behavior.

Acknowledgments

This work was partially supported by U.S. Department of Energy, Office of Energy Efficiency and Renewable Energy under grant DE-EE0007651. The authors would like to acknowledge Mark Mathias, Wenbin Gu, Roland Koestner, Anusorn Kongkanand Ratan Kukreja, Peter Harvey and Kathyrn Stevick for their support of the work.

References

1. S. Holdcroft, *Chem. Mater.*, **26** (1), 381 (2014).
2. A. Kongkanand, M. F. Mathias, *J. Phys. Chem. Lett.*, **7** (7), 1127 (2016).
3. S. Jomori et al., *J. Electrochem. Soc.*, **160** (9), F1067 (2013).
4. H. A. Gasteiger, S. S. Kocha, B. Sompalli, F.T. Wagner, *Appl. Catal. B Environ.*, **56**, 9 (2005).
5. T. Soboleva, X. Zhao, K. Malek, Z. Xie, T. Navessin, S. Holdcroft, *ACS Appl. Mater. Interfaces.*, **2** (2), 375, (2010).
6. V. Yarlagadda, M. K. Carpenter, T. E. Moylan, R. S. Kukreja, R. Koestner, W. Gu, L. Thompson, A. Kongkanand, *ACS Energy Lett.*, **3**, 618 (2018).
7. T.A. Greszler, D.A. Caulk, P. Sinha, *J. Electrochem. Soc.*, **159**, F831 (2012).
8. R. Makharia, M. F. Mathias, D. R. Baker, *J. Electrochem. Soc.*, **152** (5), A970 (2005).
9. S. Lowell, J. E. Shields, M. A. Thomas, M. Thommes, *Characterization of Porous Solids and Powders: Surface Area*, *Pore Size and Density*, p. 129, Springer, New York (2004).
10. E. Padgett et al, *J. Electrochem. Soc.*, **165** (3), F173 (2018).